

ARMY RESEARCH LABORATORY



Analysis of Projectile Penetration Into a SiC/Ti Layered Plate

by A. M. Rajendran, D. J. Grove,
and K. D. Bishnoi

ARL-TR-1364

June 1997

DTIC QUALITY INSPECTED 4

19970623 120

Approved for public release; distribution is unlimited.

The findings in this report are not to be construed as an official Department of the Army position unless so designated by other authorized documents.

Citation of manufacturer's or trade names does not constitute an official endorsement or approval of the use thereof.

Destroy this report when it is no longer need. Do not return it to the originator.

Army Research Laboratory

Aberdeen Proving Ground, MD 21005-5069

ARL-TR-1364

June 1997

Analysis of Projectile Penetration Into a SiC/Ti Layered Plate

A. M. Rajendran, D. J. Grove
Weapons and Materials Research Directorate, ARL

K. D. Bishnoi
U.S. Army Tank Automotive Research, Development, and Engineering Center

Abstract

This report describes the capabilities of the Rajendran-Grove ceramic model in predicting the depth of penetration in several layered ceramic targets. There are nine constants in the model. Five constants are adequate to describe the effects of microcracking on strength and stiffness. The variation of strength of the pulverized ceramic with respect to pressure is described through two constants. The plastic strain description involves two parameters that can be determined from a maximum stress vs. strain rate plot. A methodology to estimate these model constants is outlined in this report. Experimental data from high-velocity plate impact tests and a penetration test were employed in the calibration of the model constants for silicon carbide. Using this set of constants, the penetration of a solid tungsten rod into a layered ceramic target was analyzed. The target configuration consisted of a silicon carbide frontplate glued to a titanium backplate. The analysis showed that the simulated penetration resistance of the layered configuration was significantly influenced by the form of the ceramic model's pulverized strength equation. In addition, maintaining constant areal density, we examined the effects of different substrate materials (titanium, steel, and aluminum) on the calculated depths of penetration.

ACKNOWLEDGMENTS

The authors gratefully acknowledge the funding support of Dr. James Thompson of the U. S. Army Tank Automotive Research, Development, and Engineering Center in Warren, MI.

INTENTIONALLY LEFT BLANK

TABLE OF CONTENTS

	<u>Page</u>
ACKNOWLEDGMENTS	iii
LIST OF FIGURES	vii
1. INTRODUCTION	1
2. CONSTITUTIVE RELATIONSHIPS	1
2.1 Number of Flaws, N_o^*	3
2.2 Initial Microcrack Size, a_o	3
2.3 Coefficient of Friction, μ	3
2.4 Fracture Toughness, K_{IC}	4
2.5 Compressive Crack Growth Factor, n_1^-	4
2.6 Compressive Crack Growth Index, n_2^-	4
2.7 Post-Fracture Strength Parameters, α and β	4
3. PLATE IMPACT SIMULATIONS	6
4. DOP EXPERIMENT SIMULATIONS	6
4.1 Experimental Configuration	6
4.2 Calibration Results	9
4.3 Effect of Imposing Upper Limit on Strength of Pulverized Material	9
5. BALLISTIC PENETRATION ANALYSIS OF LAYERED TARGET PLATE	13
5.1 Baseline Penetration Configuration	13
5.2 Comparison of Results Using Two Different Equations for Pulverized Material Strength	13
5.3 Influence of Substrate Material on Calculated Penetration Depths	16
6. SUMMARY AND RECOMMENDATIONS	16
7. REFERENCES	23
DISTRIBUTION LIST	25
REPORT DOCUMENTATION PAGE	35

INTENTIONALLY LEFT BLANK

LIST OF FIGURES

<u>Figure</u>	<u>Page</u>
1. The effect of the post-fracture strength model parameter β on the computed velocity profile	5
2. A comparison between model generated and experimental velocity profiles at impact velocity 1542 m/s	7
3. EPIC finite element grid for penetration configuration (with 25.4-mm-thick ceramic tile), used to calibrate the pulverized material strength parameter β	8
4. Comparison of calculated DOP with experimental measurement for 25.4-mm-thick ceramic tile ($\beta = 0.6$)	10
5. Comparison of calculated DOP with experimental measurement for 38.1-mm-thick ceramic tile ($\beta = 0.6$)	11
6. Comparison of calculated DOP with experimental measurement for 50.8-mm-thick ceramic tile ($\beta = 0.6$)	12
7. Comparison of pulverized material strength as a function of pressure between Equation (5) ($\alpha = 0$ and $\beta = 0.6$) and Equation (6) ($\lambda = 1$ and $Y_{max} = 4$ GPa)	14
8. Baseline impact configuration for penetration analysis of layered target plate	15
9. Simulation of baseline penetration configuration using Equation (5) to describe the strength of the pulverized ceramic material ($\alpha = 0$, $\beta = 0.6$)	17
10. Simulation of baseline penetration configuration using Equation (6) to describe the strength of the pulverized ceramic material ($\lambda = 1$, $Y_{max} = 4$ GPa)	18
11. Comparison of calculated penetration depths versus time for the two different pulverized strength models	19
12. Simulation of baseline penetration configuration with steel substrate, using Equation (6) with $\lambda = 1$ and $Y_{max} = 4$ GPa	20
13. Simulation of baseline penetration configuration with aluminum substrate, using Equation (6) with $\lambda = 1$ and $Y_{max} = 4$ GPa	21

INTENTIONALLY LEFT BLANK

1. INTRODUCTION

Due to their high compressive strengths and moderate densities, ceramic materials are often employed in armor design for military vehicles. A layered armor configuration (ceramic backed by metal) tends to improve penetration resistance while maintaining structural integrity and reducing the mass of the vehicle. Typically, the armor design process relies solely on the limited data obtained from a series of trial-and-error ballistic impact experiments. This approach can be time consuming and extremely costly, depending on the number of experiments performed and the cost of manufacturing the armor target configurations. To reduce these design costs, shock wave propagation codes (hydrocodes) with advanced material models can be used to simulate some of the proposed experiments and provide preliminary evaluations of the various armor configurations. Of course, the usefulness of the code analysis is directly related to the accuracy of the material models used to describe the target materials' dynamic responses to ballistic impact.

Hydrocodes have become important design tools in armor/antiarmor design calculations. The shock and high strain rate response of materials are described through constitutive/failure and equation of state equations. In recent years, several constitutive/damage models [1-5] have been proposed and developed to describe the impact response of ceramic materials. One of them is a scalar-damage based ceramic model reported by Rajendran [5]. A brief description of the model is presented in this report. This model has been successfully implemented in the 1995 version of the EPIC finite element code [6].

In the Rajendran-Grove ceramic failure model [5], the parameters used to describe the microcrack evolution process can be determined indirectly using stress and/or particle velocity profiles from ceramic plate impact experiments. Using a shock wave propagation code, each experiment is simulated, and the microcracking constants are adjusted until the numerical results compare well with the experimental data. However, the data from this one-dimensional (uniaxial strain) configuration fails to provide information concerning the compressive strength of the pulverized ceramic material. Ballistic penetration experiments, wherein a ceramic target plate is confined laterally and backed by a thick steel plate, provide depth-of-penetration (DOP) data that can be used to calibrate the model parameter that controls the compressive strength of the pulverized ceramic material. We investigated the penetration resistance of layered targets consisting of silicon carbide backed by either titanium, steel, or aluminum.

2. CONSTITUTIVE RELATIONSHIPS

The stress-strain equations for the microcracked aggregate material are given by,

$$\sigma_{ij} = M_{ijkl} \epsilon_{kl}^e \quad (1)$$

The components of the stiffness tensor M are derived by Margolin [7]. The pressure is calculated through the Mie-Gruneisen equation of state. For porous ceramics, the intact bulk and shear moduli are corrected for porosity using Mackenzie's correction factors [8]. In the ceramic model, microcrack damage is measured in terms of a dimensionless microcrack density γ , which is defined as

$$\gamma = N_o^* a^3 \quad (2)$$

N_o^* is the average number of microflaws per unit volume, and a is the maximum microcrack size which is treated as an internal state variable. The microcracks extend when the stress state satisfies a generalized Griffith criterion [9,10]. This criterion permits microcrack extension under all three crack growth modes. In the Griffith criterion for shear crack extension [10], the dynamic coefficient of friction, μ , appears as a model constant. As Equation (2) indicates, microcrack extension causes the microcrack density γ to increase, which results in stress relaxation in the cracked ceramic material. Since N_o^* is assumed to be a constant in the model, any increase in γ is entirely due to increase in the crack size. It is possible to modify the model to allow for the evolution of N_o^* .

The damage evolution law is derived from a fracture mechanics based relationship for a single crack propagating under dynamic loading conditions, and the law is described by

$$\dot{a}_{\max} = n_1 C_R \left[1 - \left(\frac{G_c}{G_I} \right)^{n_2} \right] \quad (3)$$

where C_R is the Rayleigh wave speed, G_c is the critical strain energy release rate, and G_I is the applied strain energy release rate. The model parameters n_1 and n_2 are employed to limit the microcrack growth rate. For mode I crack opening (tensile loading), n_1 and n_2 are both assumed to be 1. However, since the microcrack growth rate tends to be lower during compressive loading (mode II), a different set of parameters, n_1^- and n_2^- , must be calibrated for this case.

Shockey et al. [11] and Curran et al. [12] address many of the deformation mechanisms in confined ceramics under ballistic impact loading conditions. These studies clearly established the presence of dislocations and twinning in the brittle ceramics due to high pressures and high strain rate loading conditions. The following strength model is used to describe plastic flow in ceramics during high strain rate loading:

$$Y = A (1 + C \ln \dot{\epsilon}^*) \quad (4)$$

where A is the initial yield strength, C is the strain rate sensitivity parameter, and $\dot{\epsilon}^*$ is the normalized equivalent plastic strain rate. A is assumed to be equal to the compressive strength at HEL (Y_{HEL}). C is calibrated by matching the shape of the plastic portion of the shock wave profile.

In the Rajendran-Grove model, the comminuted ceramic strength (Y_p) varies with confinement pressure (P). The compressive strength of the pulverized ceramic is described by the following Mohr-Coulomb type relationship:

$$Y_p = \alpha + \beta P \quad (5)$$

where α is the minimum strength and β is the slope of the linear strength-pressure relationship above α . To simplify the calibration scheme, α is generally assumed to be zero; in this case, the post-fracture strength of the ceramic is directly proportional to the applied pressure. Since the one dimensional plate impact experimental configuration is relatively insensitive to β , the calibration of this model parameter requires a series of finite element simulations of a ballistic penetration experiment involving a laterally confined ceramic target plate.

In summary, there are six microcrack model constants: N_o^* , a_o , μ , K_{IC} , n_1^- , and n_2^- . Direct measurements of N_o^* , a_o , μ , n_1^- , and n_2^- from impact experiments or from photomicrographs are, in general, very difficult or not feasible. Therefore, suitable values were determined from plate impact experiment simulations. The following subsections discuss the effects of the various ceramic model parameters on the simulated velocity profiles from a silicon carbide (SiC) plate impact test configuration.

2.1 Number of Flaws, N_o^* . Three simulations were considered using values of 10^{11} , 10^9 , and $10^7 m^{-3}$ for N_o^* . The value of 10^7 did not produce complete spall fracture. The intermediate value of 10^9 produced minimal compressive cracking followed by complete spall due to tensile cracking. The high value of 10^{11} caused excessive damage under compression, significantly affecting the loading portion of the computed velocity profile. Based on these simulations, $10^9 m^{-3}$ seems to be a reasonable value for N_o^* to cause spall without excessive compressive damage.

2.2 Initial Microcrack Size, a_o . To investigate the effect of initial microcrack size on ceramic fracture, three plate impact simulations with a_o values of 0.1 micrometer (μm), 0.2 μm , and 0.5 μm were considered. In these simulations, μ was 0.1 and N_o^* was $10^9 m^{-3}$. No microcracking occurred for values of a_o less than or equal to 0.1 μm . Partial spall occurred with $a_o = 0.2 \mu m$, and initial crack sizes greater than 0.35 μm induced complete spall in the target. The influence of a_o on the velocity profile varies with different combinations of μ and N_o^* . For silicon carbide, a_o was calibrated to be 0.5 μm .

The modeling of low velocity (below HEL) experiments required a larger value ($>10 \mu m$) for a_o to match the spall signal. Using a single value for a_o , Rajendran and Dandekar [13] reproduced the measured wave profiles (below and above HEL).

2.3 Coefficient of Friction, μ . Several simulations were performed to investigate this influence. The value for this parameter is closely tied to the values chosen for some of the other model constants, especially the compressive crack growth factor n_1^- . For instance, the effect of μ was insignificant for $n_1^- = 0.1$, whereas the effect became significant for $n_1^- = 0.2$.

In the simulations, lower values of μ tended to cause premature microcracking while the shock amplitude was still increasing during the "plastic" wave ramp. Since the compressive microcracking occurred well above the threshold level of "complete spall (under tension)," the influence of μ on the spall signal was negligible. This study suggests that a minimum value which will not cause any premature compressive damage shall be assigned to μ . In fact, this minimum value will allow the independent

determination of the other constants. When calibrating the model constants for SiC, a value of 0.1 was assumed for μ .

2.4 Fracture Toughness, K_{IC} . The ceramic model does not contain a microflaw nucleation model. Flaws are assumed to exist in the virgin ceramic material and are activated when the stress state satisfies the Griffith criterion for an initial flaw of size a_0 . Values of K_{IC} between 1 and 20 MPa \sqrt{m} did not show any effect on the wave profiles. Based on handbook values, a static fracture toughness (K_{IC}) of 4 MPa \sqrt{m} was assumed for SiC.

2.5 Compressive Crack Growth Factor, n_1^- . This model constant limits the microcrack growth rate (see Equation (3)) under compression to $n_1^- C_R$. When the Griffith criterion is satisfied for a given stress state, the time dependent microcrack extension controls the rate at which the elastic moduli are degraded. This degradation affects the shock wave speed and this, in turn, affects the pulse duration. Unfortunately, the limiting dynamic crack propagation velocity under mode II (crack sliding) conditions cannot be experimentally measured.

Based on plate impact simulations, values of n_1^- lower than 0.1 did not introduce any further change in the velocity profile. Increasing n_1^- to 0.2 widened the pulse width due to elastic moduli degradation. The shock amplitude diminished as the compressive microcracking increased with increasing n_1^- . The spall rebound portion of the velocity profile was not significantly affected by the n_1^- variations. Thus, n_1^- was assumed to be 0.1.

2.6 Compressive Crack Growth Index, n_2^- . To evaluate the effect of n_2^- on the velocity profile, several simulations were performed. The results showed that the computed profiles were unaffected by n_2^- . Since the ratio between G_c and G_I is very small at impact velocities above 1 km/s, varying this index between 0.001 and 1 did not alter the ceramic response. Two additional simulations at lower velocities also produced very similar wave profiles. Therefore, we set n_2^- equal to 1.0 for SiC.

However, this index does influence the computed stress history in a ceramic rod due to an impact by a similar rod at low velocity. In the rod-on-rod configuration, the stress state is uniaxial and the strain state is multiaxial, whereas in the plate impact configuration, the stress state is multiaxial and the strain state is uniaxial.

2.7 Post-Fracture Strength Parameters, α and β . The plate impact experimental configuration seems to be insensitive to these parameters. The simulations with three different values of β showed hardly any effect on the computed velocities profiles as can be seen in Figure 1. The average spall signal between points E and F in the figure is almost the same for the three values. Also, the computed velocity profiles for $\alpha = 1, 5, \text{ and } 10$ kbars were nearly identical to those shown in Figure 1. Therefore, in the microcrack model constant calibration scheme, α was set to 0 and β was set to 1.

POST FRACTURE STRENGTH EFFECT

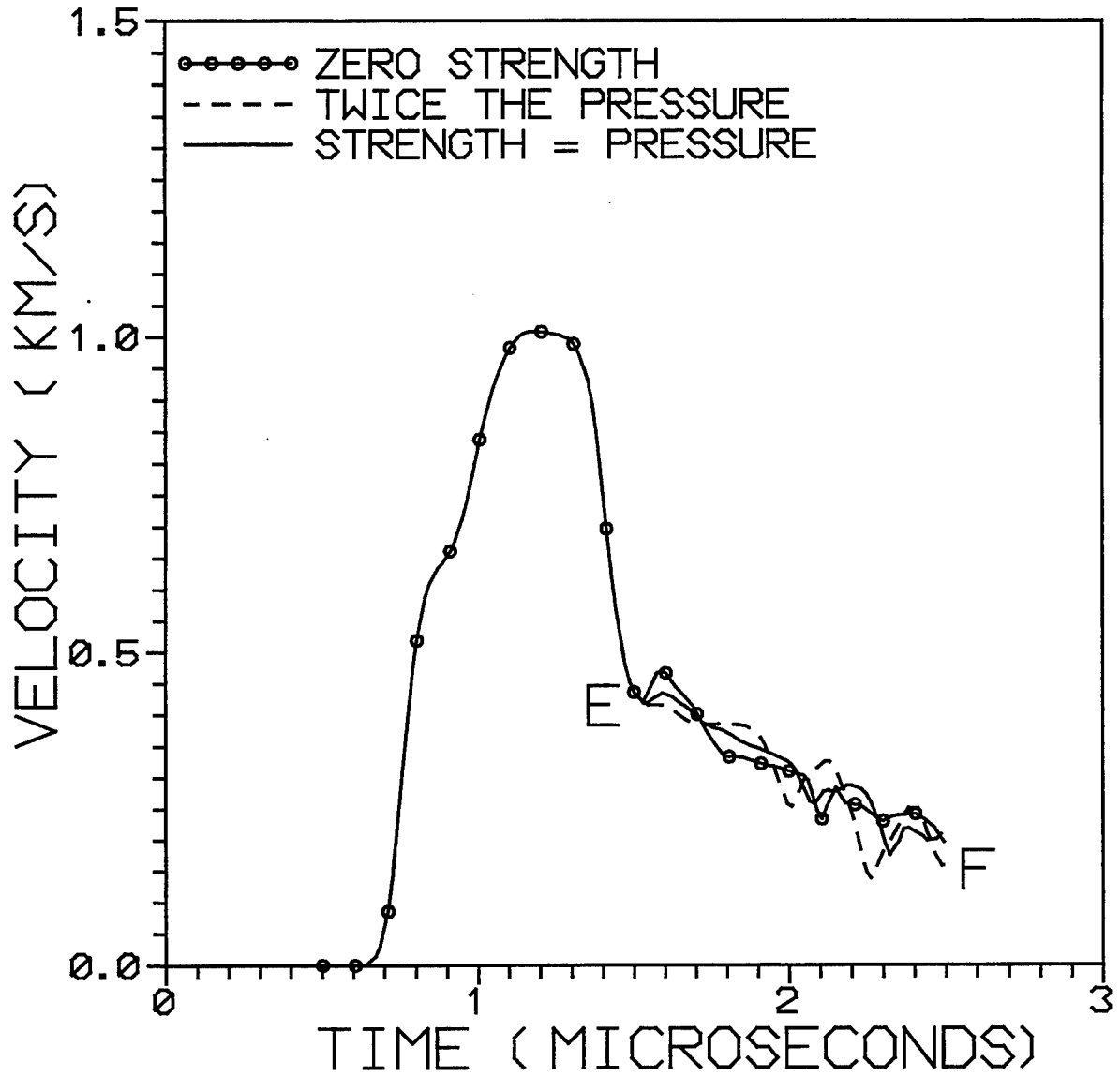


Figure 1. The effect of the post-fracture strength model parameter β on the computed velocity profile.

3. PLATE IMPACT SIMULATIONS

The model parameter calibration procedure described in the previous section employed data from the high-velocity SiC plate impact experiments reported by Kipp and Grady [14]. Figure 2 compares the EPIC code generated velocity versus time with the measured profile from the lower velocity plate impact experiment ($v = 1542$ m/s). The model reproduced all the salient features of the data.

A higher velocity (2100 m/s) plate impact experiment was also simulated using the same set of values for the model constants. The predicted velocity profile matched the data extremely well [15].

4. DOP EXPERIMENT SIMULATIONS

We also considered a penetration configuration wherein a SiC ceramic tile is laterally confined by a steel frame that is mechanically clamped to a thick steel backup plate. The projectile is a long tungsten rod ($L/D = 10$). EPIC95 code simulations of this penetration experiment were performed using the Rajendran-Grove ceramic failure model. Based on this analysis, the pulverized ceramic strength constant β was calibrated to match the measured DOP for one ceramic tile thickness. Using the same set of parameters, the ceramic model successfully predicted the measured DOP for two other ceramic tile thicknesses.

While the parameter β did not influence the velocity profiles from plate impact simulations, it did significantly influence the results of the DOP simulations. Therefore, using the microcracking model parameters determined from plate impact data, penetration simulations can be used to calibrate the ceramic model's pulverized strength parameter β .

4.1 Experimental Configuration. The penetration experiment configuration consisted of a square silicon carbide tile confined laterally by a steel frame. The entire target assembly was mechanically clamped to a thick steel backup plate. The ceramic tiles were 152.4 mm wide, and three different tile thicknesses were investigated: 25.4, 38.1, and 50.8 mm. The projectile was a tungsten rod, 79 mm long and 7.9 mm in diameter ($L/D = 10$), with an impact velocity of 1500 m/s. The experimental data consisted of the rod's DOP into the backup plate.

We used the two-dimensional (2D) axisymmetric option in EPIC to approximate the above geometry. With this assumption, the target plates and confinement frame were modeled as being circular instead of square. In the simulations, the Rajendran-Grove model described the dynamic response of the ceramic, while standard EPIC material models were used to describe the behavior of the tungsten rod and the steel backup plate. Figure 3 shows the configuration for the 25.4-mm-thick ceramic tile.

SILICON CARBIDE ($V = 1.542 \text{ KM/SEC}$)

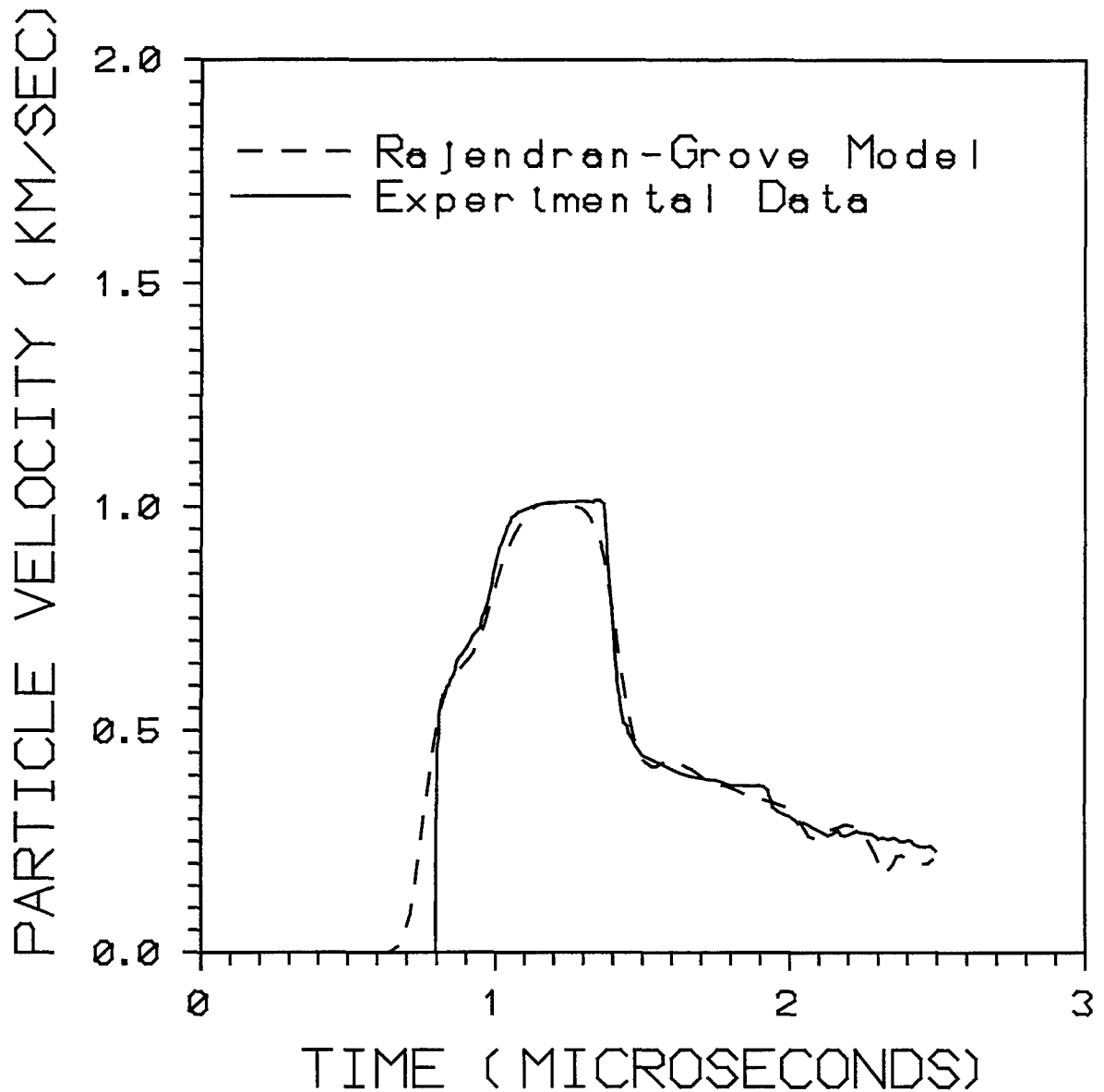


Figure 2. A comparison between model generated and experimental velocity profiles at impact velocity 1542 m/s.

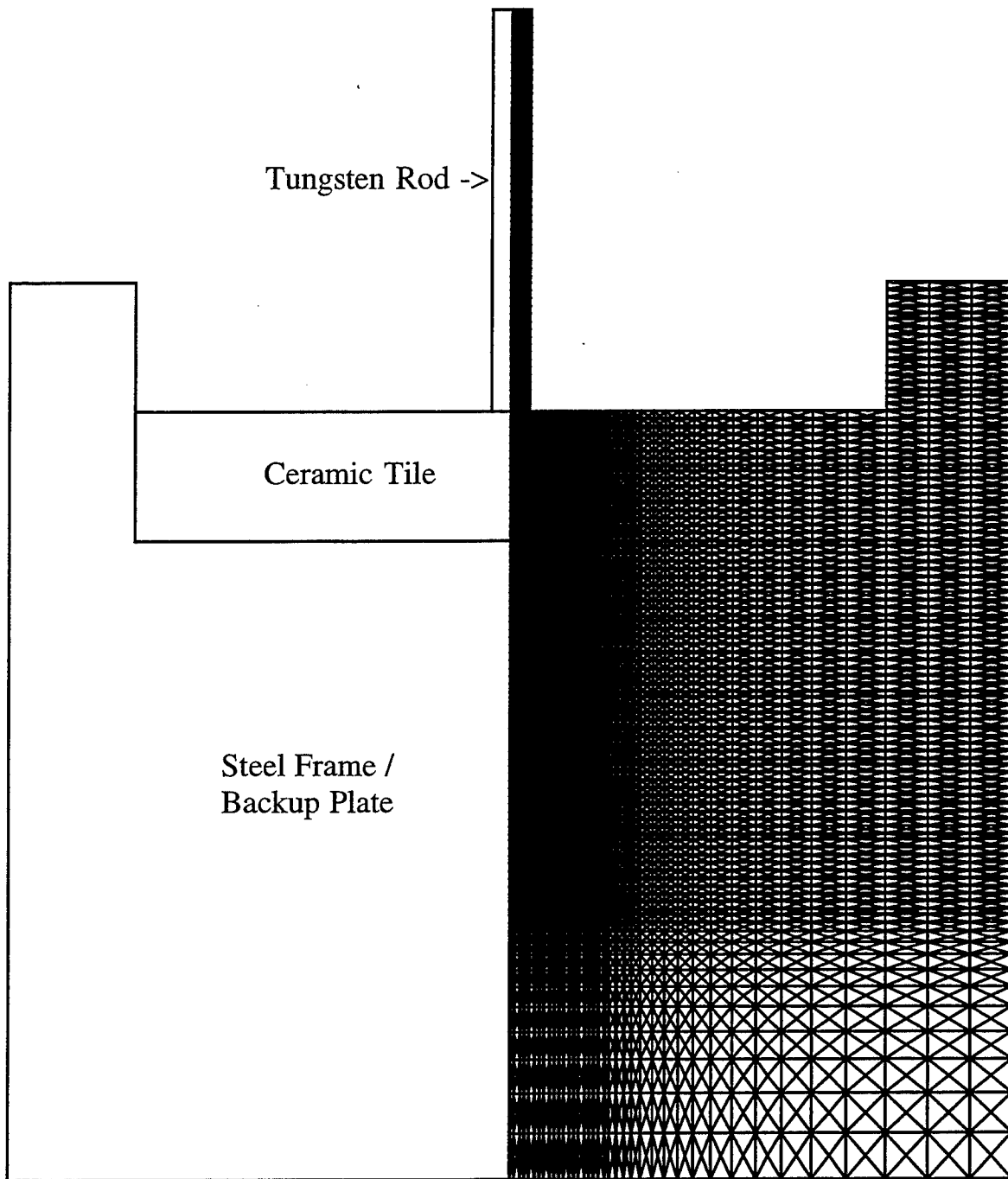


Figure 3. EPIC finite element grid for penetration configuration (with 25.4-mm-thick ceramic tile), used to calibrate the pulverized material strength parameter β .

4.2 Calibration Results. The Rajendran-Grove model employs a generalized Griffith criterion to initiate microcrack growth under both tensile and compressive stress states. In this model, the crack density (a state variable) increases as the microcracks extend. When the crack density reaches a critical value, the damaged ceramic material is assumed to pulverize (under compression). After pulverization, the material has no tensile strength, and its compressive strength is governed by Equation (5).

Based on velocity profiles from high-velocity plate impact experiments, the model parameters that characterize the growth of microcracks had previously been determined for silicon carbide [15,16]. Unfortunately, as subsection 2.1 indicates, the pulverized strength parameter β cannot be determined from plate impact experimental data. We calibrated β by adjusting it until the simulated DOPs matched the experimental results. It is important to note that the microcrack evolution parameters can also significantly affect the ceramic target's simulated penetration resistance. For this study, however, we employed the values of those parameters that had been determined from the plate impact data.

For $\beta = 1$ ($Y_p = P$), the calculated penetration depths were significantly less than the experimental measurements. With no upper bound on the strength of the pulverized material, its penetration resistance was apparently unrealistically high. Reducing β to a value of 0.6 resulted in very good agreement between the simulated and measured DOP data, as shown in Figures 4-6. The dashed lines in these figures indicate the experimentally measured DOPs.

4.3 Effect of Imposing Upper Limit on Strength of Pulverized Material. When Equation (5) is used to describe the compressive strength of the pulverized ceramic material, the strength is permitted to increase (without bound) as the pressure increases. Such behavior may be reasonable for lower pressures. However, for very high-velocity penetration configurations, the pressures at the projectile/target interface can become extremely high. Intuitively, there must be a limiting value for the compressive strength of the pulverized ceramic; certainly it must be lower than that of the intact ceramic material. Accordingly, the Johnson-Holmquist constitutive model for brittle materials [4] defines a strain rate dependent maximum strength for the fractured material.

To investigate the effect of imposing an upper limit on the strength of the pulverized ceramic material, we implemented the following simple expression in the Rajendran-Grove model to describe the compressive strength of the post-fractured material:

$$Y_p = \min[Y_{max}, (\lambda P)] \quad , \quad (6)$$

where Y_{max} and λ are model parameters. Y_{max} is a constant that defines the upper limit on the strength of the pulverized material, and λ is the slope of the linear strength-pressure relationship below Y_{max} .

Using this modified Rajendran-Grove ceramic failure model, we calibrated Y_{max} and λ to match the DOP data. To simplify this procedure, λ was assumed to be equal to 1; the optimum value for Y_{max} was found to be 4 GPa. The computed DOPs were almost identical to those illustrated in Figures 4-6.

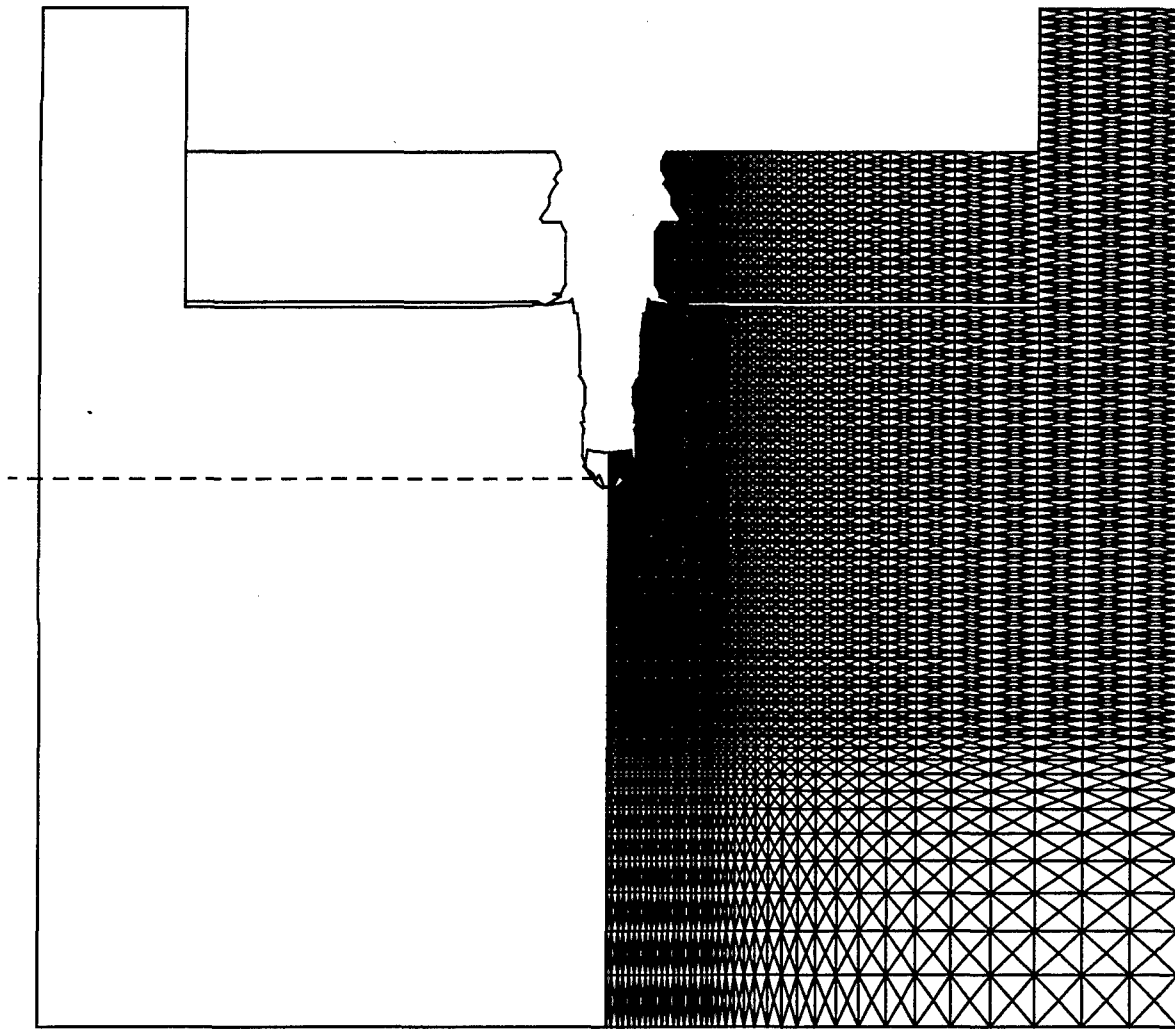


Figure 4. Comparison of calculated DOP with experimental measurement for 25.4-mm-thick ceramic tile ($\beta = 0.6$).

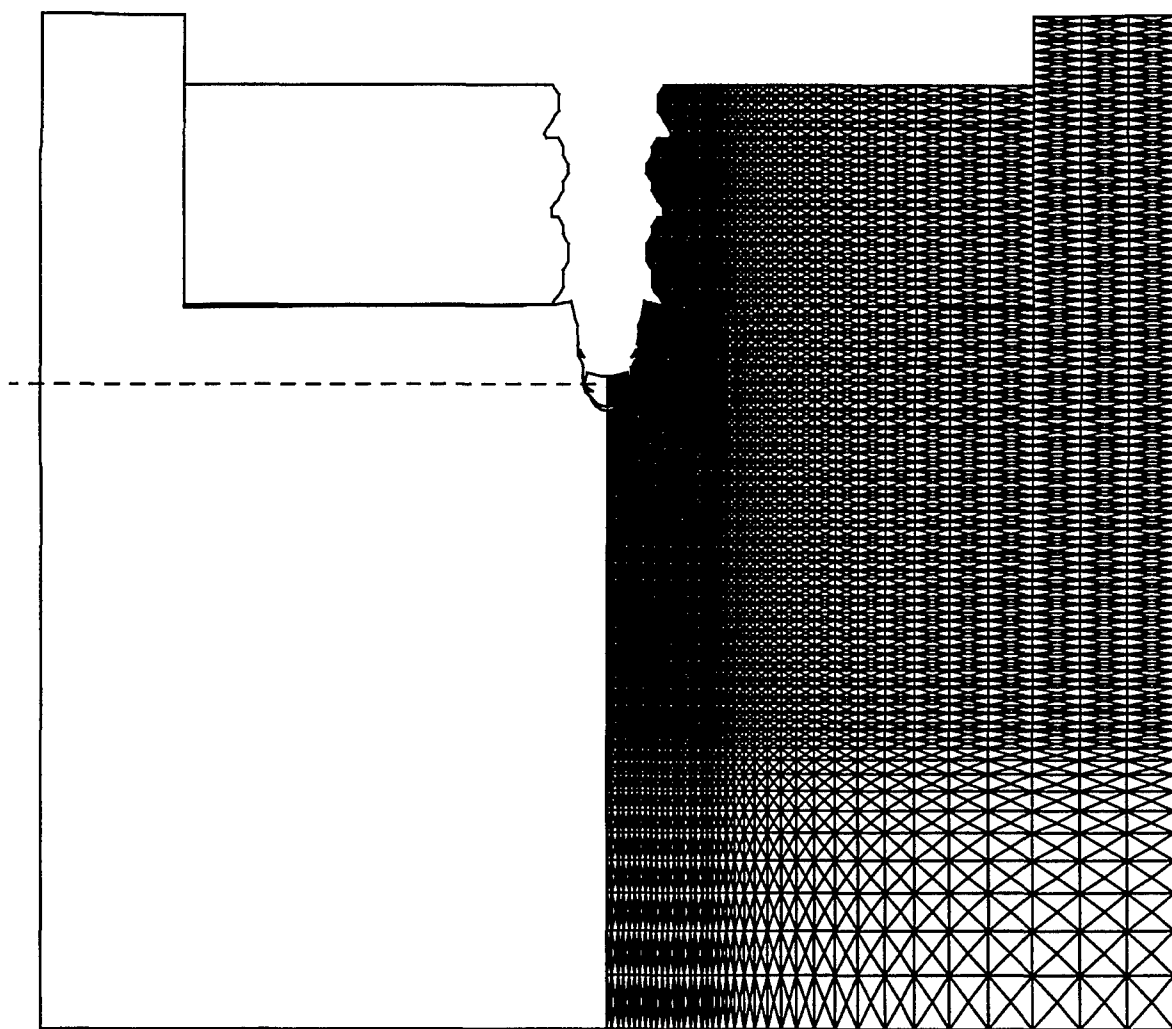


Figure 5. Comparison of calculated DOP with experimental measurement for 38.1-mm-thick ceramic tile ($\beta = 0.6$).

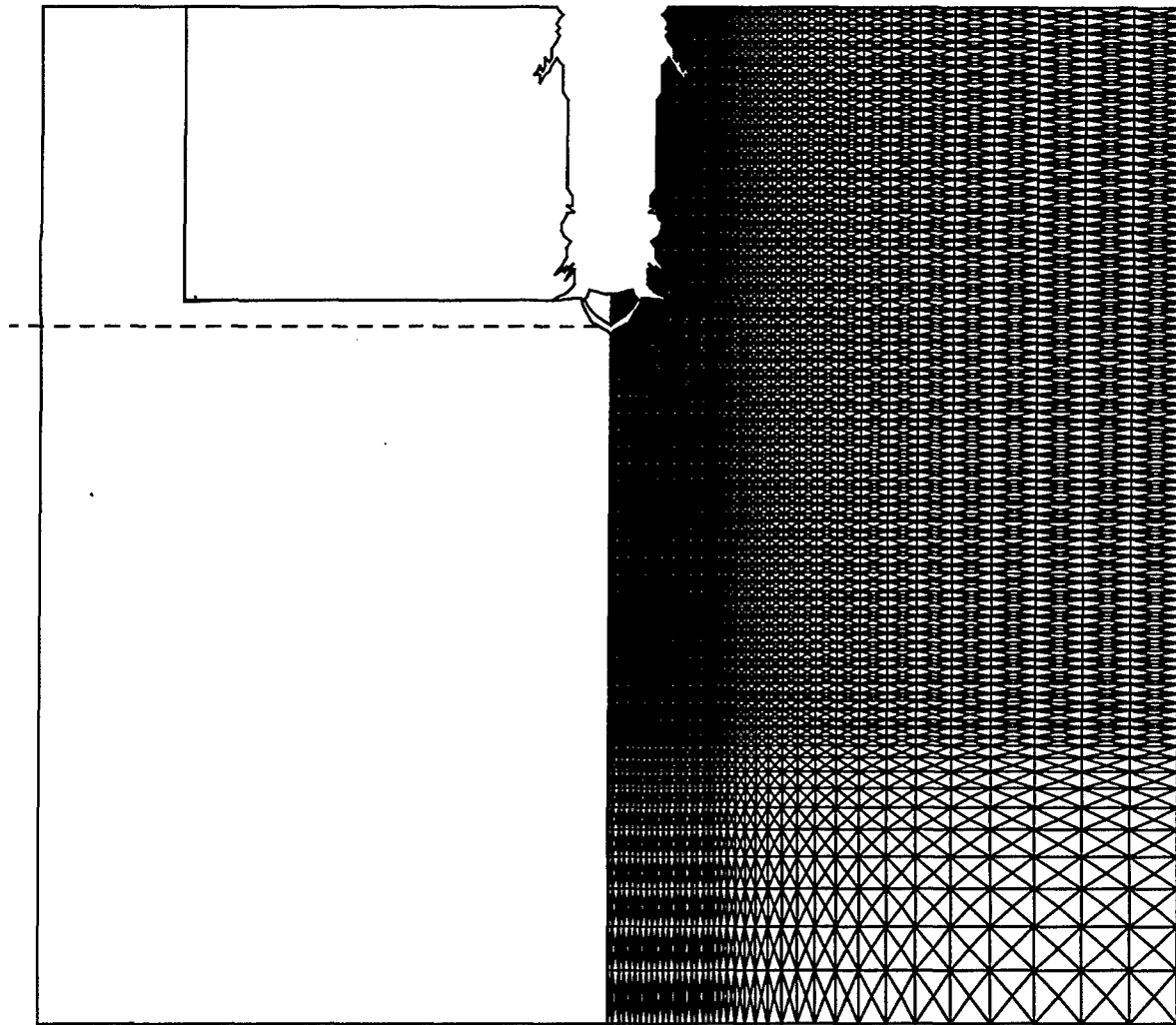


Figure 6. Comparison of calculated DOP with experimental measurement for 50.8-mm-thick ceramic tile ($\beta = 0.6$).

Using the calibrated values for β and Y_{max} , Figure 7 compares Equations (5) and (6). In this figure, the dashed (Equation (5)) and solid (Equation (6)) lines indicate how strength varies with pressure for the two expressions. At lower pressures (below 6.67 GPa), Equation (5) predicts significantly lower strength for the confined ceramic powder. Beyond 6.67 GPa, the expression predicts continuously increasing strength with increasing pressure; this means that the material's penetration resistance will also increase indefinitely with the pressure. Equation (6), on the other hand, predicts higher strength for the pulverized material at lower pressures, and then imposes a limit on the strength at higher pressures. This strength model, which also limits the penetration resistance of the confined ceramic powder, seems more appropriate for describing the penetration process in a confined ceramic target.

5. BALLISTIC PENETRATION ANALYSIS OF LAYERED TARGET PLATE

Using EPIC95 and the Rajendran-Grove ceramic failure model to describe the dynamic response of the ceramic material, we simulated a ballistic penetration configuration involving a silicon carbide front plate glued to a titanium backplate. Using previously calibrated ceramic model constants for silicon carbide [15-17], we investigated the influence of the pulverized material strength model on the target's penetration resistance. In addition, maintaining constant areal density, we investigated the effects of replacing the titanium substrate material with steel and aluminum.

5.1 Baseline Penetration Configuration. The baseline penetration configuration consisted of a circular silicon carbide plate glued to a circular titanium backplate. Both target plates were 152.4 mm in diameter; the ceramic plate was 28.575 mm thick, and the titanium plate was 25.4 mm thick. The projectile was a 214-g tungsten rod, 52.4 mm long and 17 mm in diameter ($L/D \approx 3$), with an impact velocity of 1149 m/s.

We used the 2D axisymmetric option in EPIC to model the above geometry. The bond between the two plates was modeled as infinite cohesion; one continuous grid was used to describe the target. Also, the edges of the target plates were assumed to be rigidly clamped. In the simulations, the Rajendran-Grove model described the dynamic response of the silicon carbide, while standard EPIC material models were used to describe the behavior of the tungsten rod and the titanium backup plate. Figure 8 shows the baseline configuration.

5.2 Comparison of Results Using Two Different Equations for Pulverized Material Strength. Subsection 4.3 indicated that both pulverized strength expressions (see Equations (5) and (6)) could be calibrated to match DOP data from ballistic penetration experiments involving laterally confined ceramic tiles backed by thick steel plates. The calibrated values for the Equation (5) parameters were $\alpha = 0$ and $\beta = 0.6$, while those for Equation (6) were $\lambda = 1$ and $Y_{max} = 4$ GPa. Both pulverized strength equations produced nearly identical calculated DOPs for each of three different ceramic tile thicknesses. Equation (6), which limits the penetration resistance of the confined ceramic powder, seems more appropriate for describing the penetration process in a confined ceramic target.

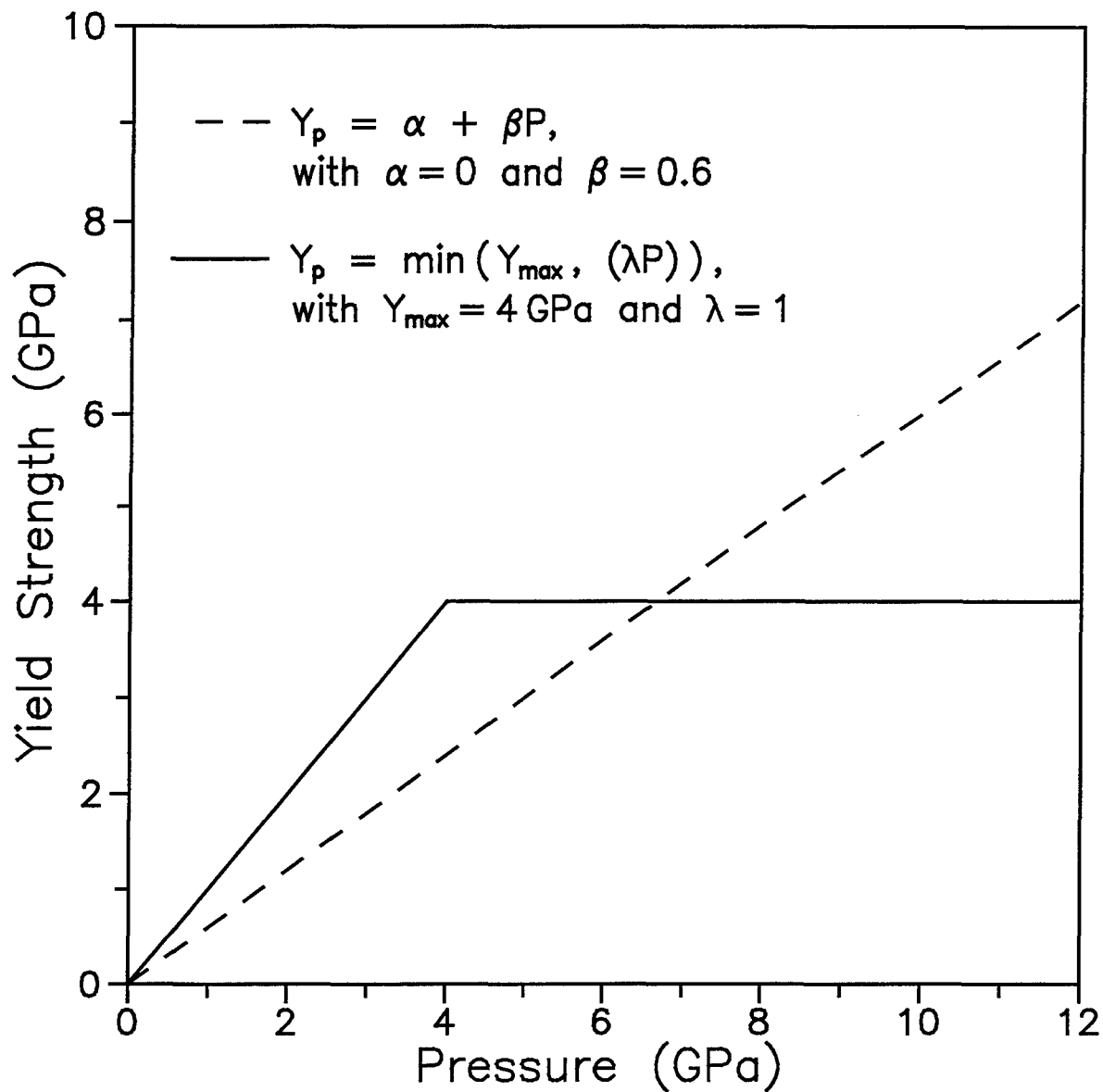


Figure 7. Comparison of pulverized material strength as a function of pressure between Equation (5) ($\alpha = 0$ and $\beta = 0.6$) and Equation (6) ($\lambda = 1$ and $Y_{\max} = 4$ GPa).

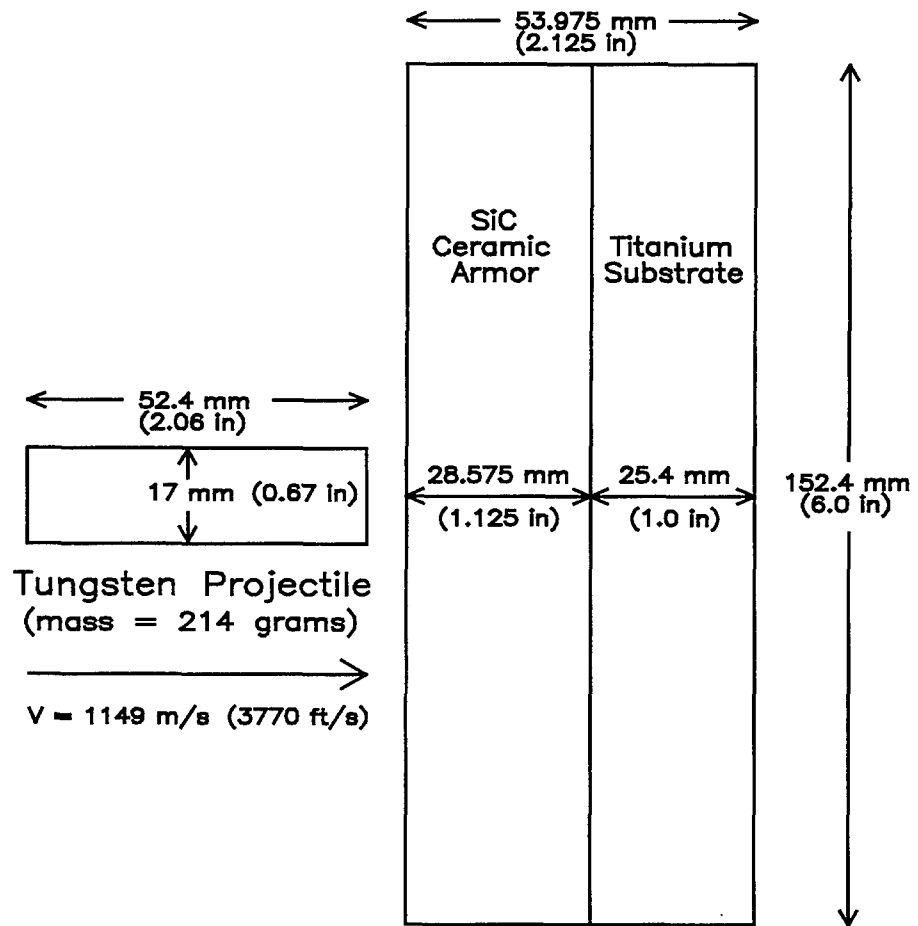


Figure 8. Baseline impact configuration for penetration analysis of layered target plate.

To investigate the sensitivity of the layered target configuration to the form of the pulverized strength equation, the baseline penetration configuration (see Figure 8) was simulated using both Equations (5) and (6) with the calibrated parameters from references [15-17]. As Figures 9 and 10 illustrate, Equation (5) predicted a complete perforation of the target (exit velocity ≈ 209 m/s), while Equation (6) predicted only partial penetration with a permanent bulge in the titanium substrate.

At lower pressures, Equation (6) predicts higher pulverized material strengths than Equation (5). Apparently, the corresponding increase in penetration resistance is sufficient to defeat the projectile. Figure 11 compares the penetration depths versus time from the two simulations; the dashed line corresponds to Equation (5), while the solid line represents Equation (6). The two profiles are identical during the first 15 μ s. After the ceramic material begins to pulverize, however, the influence of the pulverized strength equation becomes apparent. The simulation that employed Equation (6) predicted greater erosion and deceleration rates in the penetrating rod due to the higher strength of the pulverized ceramic material.

5.3 Influence of Substrate Material on Calculated Penetration Depths. Using Equation (6) to describe the strength of the pulverized ceramic material, we investigated the influence of the substrate material on the calculated penetration process. To accomplish this, the baseline penetration configuration was simulated with RHA steel and 6061-T6 aluminum backplates.

For comparison purposes, we maintained constant areal density in the layered target plate. In the baseline configuration, the areal densities of the ceramic and titanium plates were about 91 kg/m² (18.6 psf) and 112 kg/m² (23 psf), respectively, for a total areal density of 203 kg/m² (41.6 psf). This areal density required a steel substrate thickness of about 14.4 mm and an aluminum substrate thickness of about 41.6 mm in the EPIC simulations. As Figures 12 and 13 show, the steel substrate performed as well as the titanium, but the aluminum substrate was unable to stop the rod (exit velocity ≈ 570 m/s).

6. SUMMARY AND RECOMMENDATIONS

The Rajendran-Grove ceramic failure model was successfully implemented in the 1995 version of EPIC. The modified EPIC code was subsequently used to simulate an experimental configuration consisting of a long tungsten rod penetrating a silicon carbide ceramic tile that was laterally confined and backed by a massive steel holder. Employing previously determined model parameters to describe the evolution of microcrack damage in the ceramic, the model's pulverized strength parameter was calibrated to match the experimentally measured DOP data for three different ceramic tile thicknesses.

The pulverized strength equation was then revised to include an upper limit, or "cap," on the strength of the post-fractured material. After calibration, this new model predicted penetration depths nearly identical to those of the original pulverized strength model.

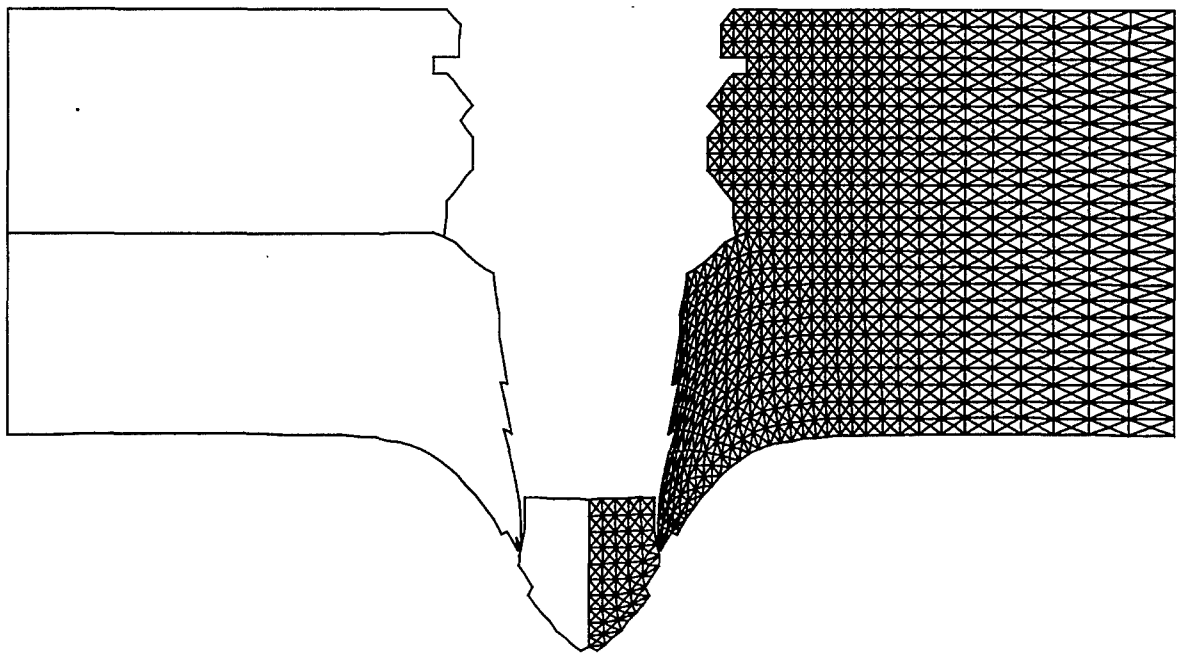


Figure 9. Simulation of baseline penetration configuration using Equation (5) to describe the strength of the pulverized ceramic material ($\alpha = 0$, $\beta = 0.6$).

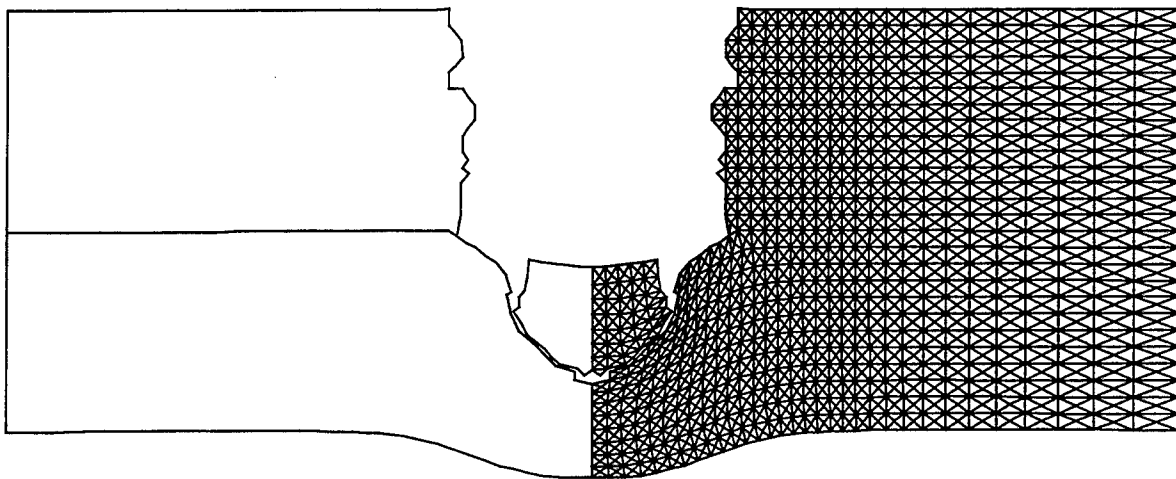


Figure 10. Simulation of baseline penetration configuration using Equation (6) to describe the strength of the pulverized ceramic material ($\lambda = 1$, $Y_{max} = 4$ GPa).

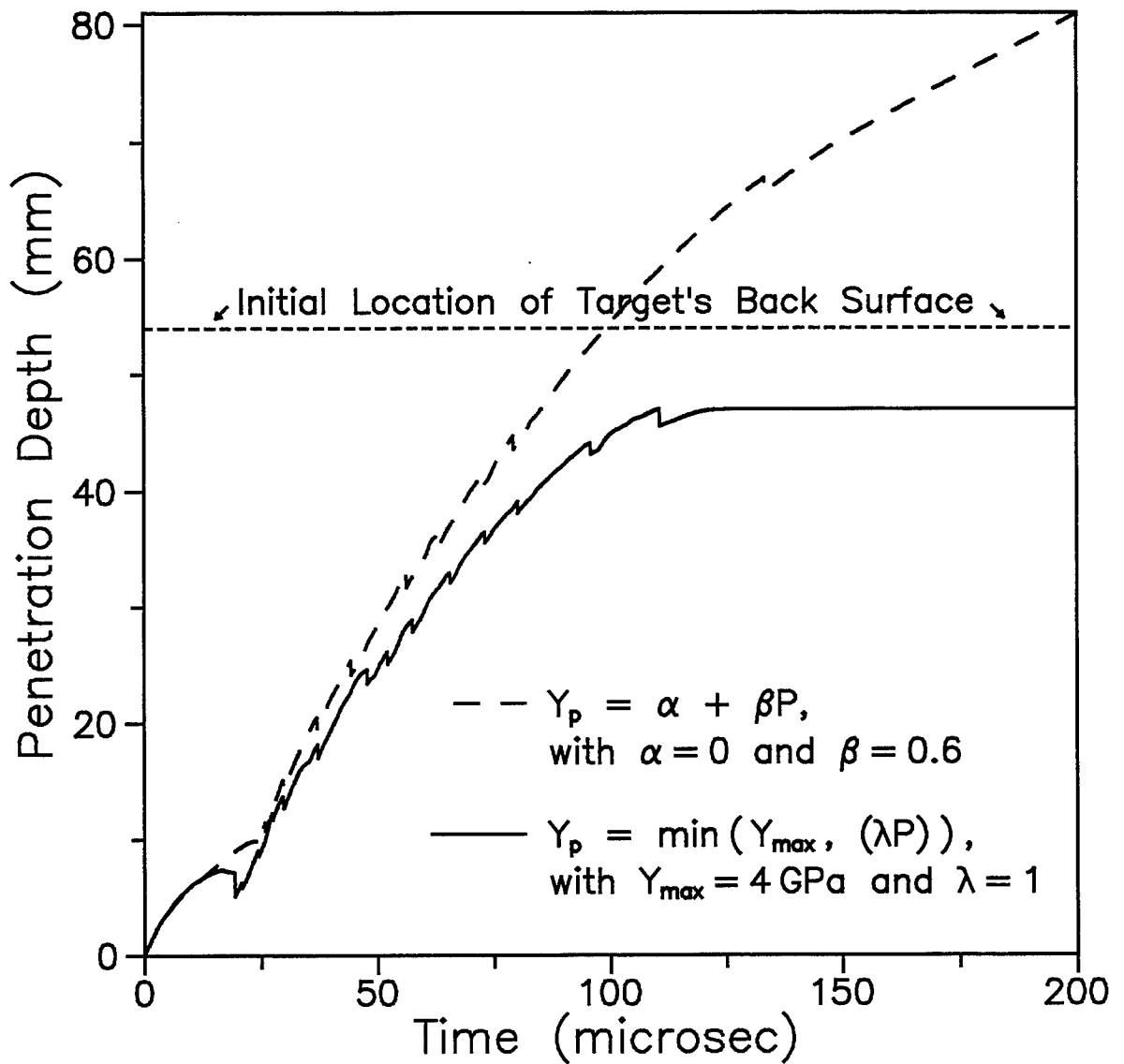


Figure 11. Comparison of calculated penetration depths versus time for the two different pulverized strength models.

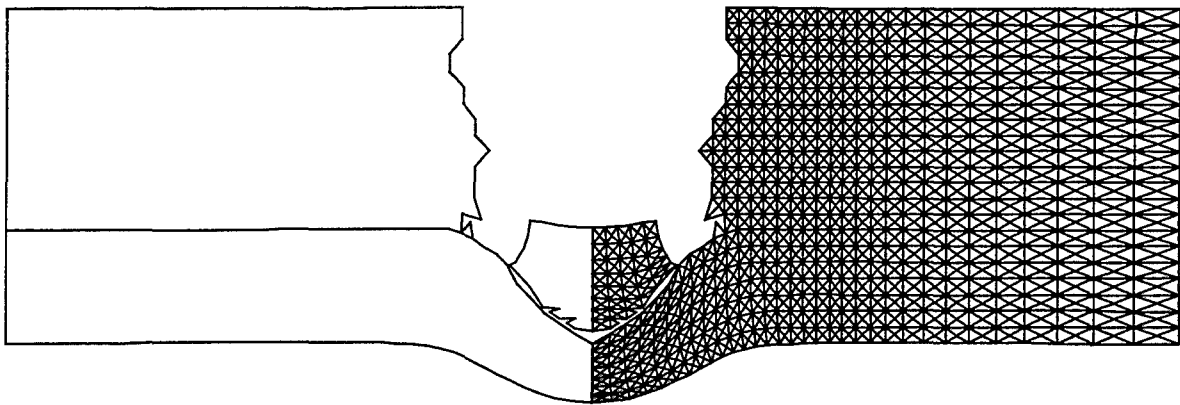


Figure 12. Simulation of baseline penetration configuration with steel substrate, using Equation (6) with $\lambda = 1$ and $Y_{max} = 4$ GPa.

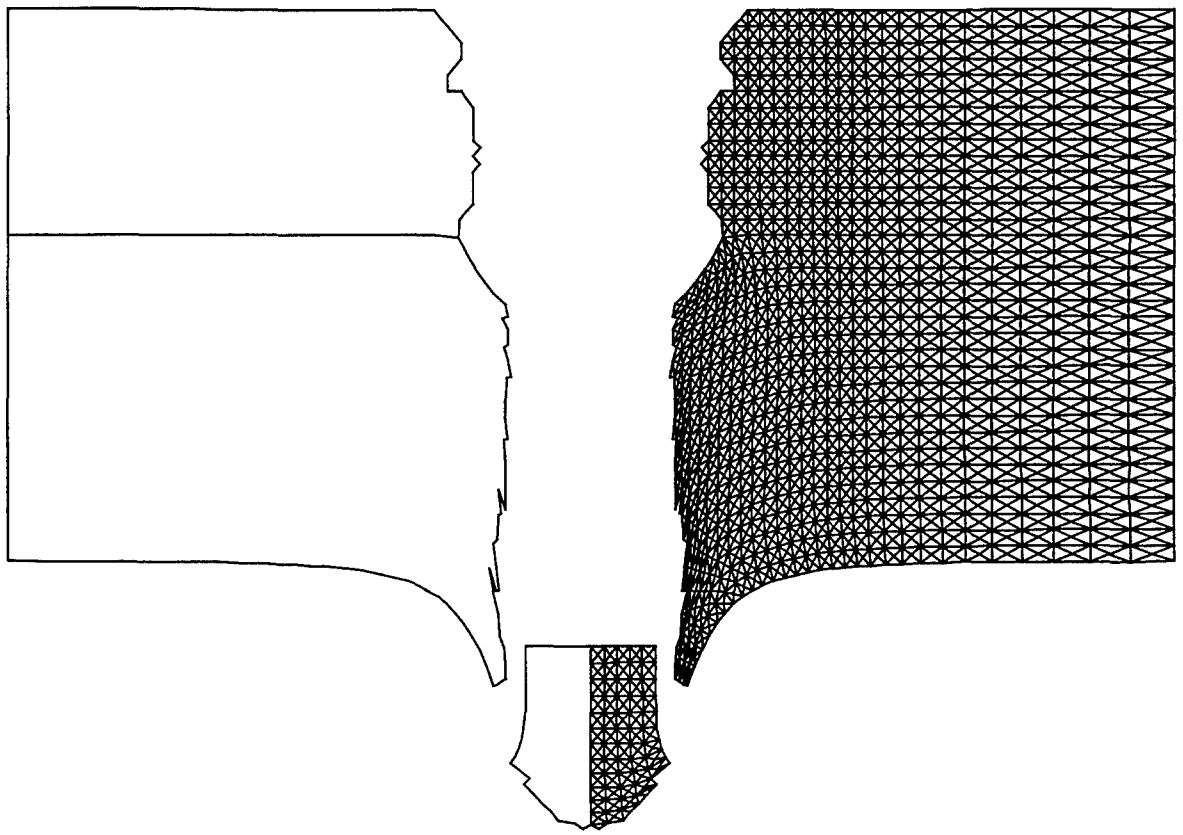


Figure 13. Simulation of baseline penetration configuration with aluminum substrate, using Equation (6) with $\lambda = 1$ and $Y_{max} = 4$ GPa.

The modified EPIC code was also used to investigate the penetration of a tungsten rod into a layered target consisting of a silicon carbide ceramic plate glued to a titanium backplate. In simulations of this penetration configuration, the Rajendran-Grove model was used to describe microcrack damage evolution in the ceramic material, and two different equations were employed to define the compressive strength of the pulverized material (as a function of pressure). Using previously calibrated parameters, the unbounded pulverized strength equation predicted significantly less penetration resistance than the bounded equation. Using the equation that imposes an upper bound on the strength of the pulverized ceramic material, the effects of substrate material on the layered target's penetration resistance were also investigated. Maintaining constant areal density in the target, the simulations predicted that a steel backing performs as well as titanium, while an aluminum backplate is unable to defeat the tungsten projectile.

Other penetration configurations should be simulated to further investigate the generality of the proposed Rajendran-Grove ceramic failure model constants. Higher penetration velocities would be useful in confirming the upper limit on the strength of the post-fractured material.

7. REFERENCES

1. Rajendran, A. M., and J. L. Kroupa, "Impact Damage Model for Ceramic Materials," *J. of Appl. Physics* **16**, pp. 3560-3565, 1989.
2. Addressio, F. L., and J. N. Johnson, "A Constitutive Model for the Dynamic Response of Brittle Materials," LA-UR-89-2651, Los Alamos National Laboratory, Los Alamos, NM, 1989.
3. Steinberg, D. J., "Computer Studies of the Dynamic Strength of Ceramics," *Shock Compression of Condensed Matter - 1991*, pp. 447-450, 1992.
4. Johnson, G. R., and T. J. Holmquist, "A Computational Constitutive Model for Brittle Materials Subjected to Large Strains, High Strain Rates, and High Pressures," in *Shock Wave and High Strain-Rate Phenomena in Materials*, 1992.
5. Rajendran, A. M., "Modeling the Impact Behavior of AD85 Ceramic Under Multiaxial Loading," *Int. J. Impact Engng.* **15**, pp. 749-768, 1994.
6. Johnson, G. R., R. A. Stryk, E. H. Petersen, T. J. Holmquist, J. A. Schonhardt, and C. R. Burns, "User Instructions for the 1995 Version of the EPIC Research Code," Alliant Techsystems Inc., 1994.
7. Margolin, L. G., "Elastic Moduli of a Cracked Body," *Int. Journal of Fracture* **22**, pp. 65-79, 1983.
8. Mackenzie, J. H., "The Elastic Constants of a Solid Containing Spherical Holes," *Proc. Phys. Soc.* **2**, p. 63, 1950.
9. Margolin, L. G., "A Generalized Griffith Criterion for Crack Propagation," *Engineering Fracture Mechanics* **19**, pp. 539-543, 1984.
10. Dienes, J. K., "Comments on 'A Generalized Griffith Criterion for Crack Propagation' by L. G. Margolin," A Technical Note, *Engineering Fracture Mechanics* **3**, pp. 615-617, 1986.
11. Shockey, D. A., D. R. Curran, L. Seaman, J. T. Rosenberg, and C. F. Petersen, "Fragmentation of Rock Under Dynamic Loads," *Int. J. Rock. Mech. Sci. and Geomech. Abstr.*, Vol. II, pp. 303-317, 1974.
12. Curran, D. R., L. Seaman, and D. A. Shockey, "Dynamic Failure of Solids," *Physics Report*, Vol. 147, pp. 253-388, 1987.
13. Rajendran, A. M., and D. P. Dandekar, "Inelastic Response of AD995 Alumina," *Int. J. Impact Engng.* **17**, pp. 649-660, 1995.
14. Kipp, M. E., and D. E. Grady, "Shock Compression and Release in High-Strength Ceramics," Sandia Report SAND89-1461, Sandia National Laboratory, NM, July 1989.
15. Grove, D. J., and A. M. Rajendran, "Modeling of Kipp-Grady Plate Impact Experiments on Ceramics Using the Rajendran-Grove Ceramic Model," in *High-Pressure Science and Technology - 1993*, pp. 749-752, 1994.

16. Rajendran, A. M., and D. J. Grove, "Determination of Rajendran-Grove Ceramic Constitutive Model Constants," in *Proceedings of the 1995 APS Shock Compression Conference*, pp. 539-542, 1996.
17. Grove, D. J., and A. M. Rajendran, "Effects of Pulverized Material Strength on Penetration Resistance of Ceramic Targets," in *Proceedings of the 1995 APS Shock Compression Conference*, pp. 1143-1146, 1996.

NO. OF
COPIES ORGANIZATION

2 DEFENSE TECHNICAL
INFORMATION CENTER
DTIC DDA
8725 JOHN J KINGMAN RD
STE 0944
FT BELVOIR VA 22060-6218

1 HQDA
DAMO FDQ
DENNIS SCHMIDT
400 ARMY PENTAGON
WASHINGTON DC 20310-0460

1 CECOM
SP & TRRSTRL COMMCTN DIV
AMSEL RD ST MC M
H SOICHER
FT MONMOUTH NJ 07703-5203

1 PRIN DPTY FOR TCHNLGY HQ
US ARMY MATCOM
AMCDCG T
M FISSETTE
5001 EISENHOWER AVE
ALEXANDRIA VA 22333-0001

1 PRIN DPTY FOR ACQUSTN HQS
US ARMY MATCOM
AMCDCG A
D ADAMS
5001 EISENHOWER AVE
ALEXANDRIA VA 22333-0001

1 DPTY CG FOR RDE HQS
US ARMY MATCOM
AMCRD
BG BEAUCHAMP
5001 EISENHOWER AVE
ALEXANDRIA VA 22333-0001

1 ASST DPTY CG FOR RDE HQS
US ARMY MATCOM
AMCRD
COL S MANESS
5001 EISENHOWER AVE
ALEXANDRIA VA 22333-0001

NO. OF
COPIES ORGANIZATION

1 DPTY ASSIST SCY FOR R&T
SARD TT F MILTON
THE PENTAGON RM 3E479
WASHINGTON DC 20310-0103

1 DPTY ASSIST SCY FOR R&T
SARD TT D CHAIT
THE PENTAGON
WASHINGTON DC 20310-0103

1 DPTY ASSIST SCY FOR R&T
SARD TT K KOMINOS
THE PENTAGON
WASHINGTON DC 20310-0103

1 DPTY ASSIST SCY FOR R&T
SARD TT B REISMAN
THE PENTAGON
WASHINGTON DC 20310-0103

1 DPTY ASSIST SCY FOR R&T
SARD TT T KILLION
THE PENTAGON
WASHINGTON DC 20310-0103

1 OSD
OUSD(A&T)/ODDDR&E(R)
J LUPO
THE PENTAGON
WASHINGTON DC 20301-7100

1 INST FOR ADVNCD TCHNLGY
THE UNIV OF TEXAS AT AUSTIN
PO BOX 202797
AUSTIN TX 78720-2797

1 DUSD SPACE
1E765 J G MCNEFF
3900 DEFENSE PENTAGON
WASHINGTON DC 20301-3900

1 USAASA
MOAS AI W PARRON
9325 GUNSTON RD STE N319
FT BELVOIR VA 22060-5582

<u>NO. OF COPIES</u>	<u>ORGANIZATION</u>
1	CECOM PM GPS COL S YOUNG FT MONMOUTH NJ 07703
1	GPS JOINT PROG OFC DIR COL J CLAY 2435 VELA WAY STE 1613 LOS ANGELES AFB CA 90245-5500
1	ELECTRONIC SYS DIV DIR CECOM RDEC J NIEMELA FT MONMOUTH NJ 07703
3	DARPA L STOTTS J PENNELLA B KASPAR 3701 N FAIRFAX DR ARLINGTON VA 22203-1714
1	SPCL ASST TO WING CMNDR 50SW/CCX CAPT P H BERNSTEIN 300 O'MALLEY AVE STE 20 FALCON AFB CO 80912-3020
1	USAF SMC/CED DMA/JPO M ISON 2435 VELA WAY STE 1613 LOS ANGELES AFB CA 90245-5500
1	US MILITARY ACADEMY MATH SCI CTR OF EXCELLENCE DEPT OF MATHEMATICAL SCI MDN A MAJ DON ENGEN THAYER HALL WEST POINT NY 10996-1786
1	DIRECTOR US ARMY RESEARCH LAB AMSRL CS AL TP 2800 POWDER MILL RD ADELPHI MD 20783-1145

<u>NO. OF COPIES</u>	<u>ORGANIZATION</u>
1	DIRECTOR US ARMY RESEARCH LAB AMSRL CS AL TA 2800 POWDER MILL RD ADELPHI MD 20783-1145
3	DIRECTOR US ARMY RESEARCH LAB AMSRL CI LL 2800 POWDER MILL RD ADELPHI MD 20783-1145
	<u>ABERDEEN PROVING GROUND</u>
2	DIR USARL AMSRL CI LP (305)

<u>NO. OF</u> <u>COPIES</u>	<u>ORGANIZATION</u>	<u>NO. OF</u> <u>COPIES</u>	<u>ORGANIZATION</u>
5	DEFENSE NUCLEAR AGENCY MAJ J LYON CDR K W HUNTER T FREDERICKSON R J LAWRENCE SPSP K KIBONG 6801 TELEGRAPH RD ALEXANDRIA VA 22310-3398	4	COMMANDER US ARMY BELVOIR RD&E CTR STRBE N B WESTLICH STRBE JMC T HANSHAW STRBE NAN S G BISHOP J WILLIAMS FORT BELVOIR VA 22060-5166
3	COMMANDER US ARMY ARDEC AMSTA AR FSA E W P DUNN J PEARSON E BAKER PICATINNY ARSENAL NJ 07806-5000	2	COMMANDER US ARMY RESEARCH OFFICE K IYER J BAILEY PO BOX 12211 RESEARCH TRIANGLE PARK NC 27709-2211
1	COMMANDER US ARMY ARDEC AMSTA AR CCH V M D NICOLICH PICATINNY ARSENAL NJ 07806-5000	1	NAVAL RESEARCH LAB A E WILLIAMS CODE 6684 4555 OVERLOOK AVE SW WASHINGTON DC 20375
1	COMMANDER US ARMY ARDEC E ANDRICOPOULOS PICATINNY ARSENAL NJ 07806-5000	1	NAVAL AIR WARFARE CTR S A FINNEGAN BOX 1018 RIDGECREST CA 93556
1	COMMANDER USA STRATEGIC DEFNS CMD CSSD H LL T CROWLES HUNTSVILLE AL 35807-3801	3	COMMANDER NAVAL WEAPONS CENTER T T YEE CODE 3263 D THOMPSON CODE 3268 W J MCCARTER CODE 6214 CHINA LAKE CA 93555
2	COMMANDER US ARMY MICOM AMSMI RD ST WF D LOVELACE M SCHEXNAYDER REDSTONE ARSENAL AL 35898-5250	1	NAVAL POST GRADUATE SCHOOL PHYSICS DEPARTMENT J STERNBERG MONTEREY CA 93943
1	MIS DEFNS & SPACE TECHNOLOGY CSSD SD T K H JORDAN PO BOX 1500 HUNTSVILLE AL 34807-3801	2	AIR FORCE ARMAMENT LAB AFATL DLJW W COOK M NIXON EGLIN AFB FL 32542

<u>NO. OF</u> <u>COPIES</u>	<u>ORGANIZATION</u>	<u>NO. OF</u> <u>COPIES</u>	<u>ORGANIZATION</u>
5	U.S. ARMY TANK AUTOMOTIVE RESEARCH DEVELOPMENT & ENGINEERING CENTER K BISHNOI AMSTA-TR-R, MS: 263 WARREN, MI 48397-5000	5	DIRECTOR LANL D MANDELL J SHANER MS F670 R DAVIDSON MS K557 J JOHNSON G787 F ADDESSIO G787 PO BOX 1663 LOS ALAMOS NM 87545
2	USAF PHILLIPS LABORATORY PL WSCD FIROOZ ALLAHDAI PV VTA D SPENCER 3550 ABERDEEN AVE SE KIRTLAND AFB NM 87117-5776	1	JET PROPULSION LAB M ADAMS IMPACT PHYSICS GROUP 4800 OAK GROVE DR PASADENA CA 91109
11	DIRECTOR SANDIA NATL LABS E S HERTEL JR MS 0819 J ASAY MS 0458 R BRANNON MS 0820 L CHHABILDAS MS 0821 D CRAWFORD MS 0821 M FURNISH MS 0821 P TAYLOR ORG 1432 M KIPP DIV 1533 P YARRINGTON DIV 1533 M FORRESTAL DIV 1551 R GRAHAM DIV 1551 PO BOX 5800 ALBUQUERQUE NM 87185-0307	3	CALTECH A INGERSOLL MS 170 25 PROF G RAVICHANDRAN T J AHRENS MS 252 21 1201 E CALIFORNIA BLVD PASADENA CA 91125
7	DIRECTOR LLNL M J MURPHY N C HOLMES W TAO L282 P URTIEW L282 A HOLT L290 J E REAUGH L290 W J NELLIS L299 PO BOX 808 LIVERMORE CA 94550	1	GEORGIA INSTITUTE OF TECHNOLOGY COMPUTATIONAL MODELING CENTER S ATLURI ATLANTA GA 30332-0356
		1	NC STATE UNIVERSITY YASUYUKI HORIE RALEIGH NC 27695-7908
		1	SOUTHWEST RESEARCH INSTITUTE C ANDERSON PO DRAWER 28510 SAN ANTONIO TX 78284
		2	UNIVERSITY OF DELAWARE DEPT OF MECHANICAL ENGINEERING PROF J GILLESPIE PROF J VINSON NEWARK DE 19716

<u>NO. OF COPIES</u>	<u>ORGANIZATION</u>
1	VIRGINIA POLYTECHNIC INSTITUTE COLLEGE OF ENGINEERING R BATRA BLACKSBURG VA 24061-0219
1	ADVANCED TECHNOLOGY INC J ADAMS PO BOX 125 DAHLGREN VA 22448-0125
1	ALLIANT TECHSYSTEMS INC G R JOHNSON MN11 2925 600 SECOND ST NE HOPKINS MN 55343
1	COMPUTATIONAL MECHANICS CONSULTANTS J A ZUKAS PO BOX 11314 BALTIMORE MD 21239-0314
2	INST OF ADVANCED TECHNOLOGY UNIVERSITY OF TX AUSTIN S J BLESS T M KIEHNE 4030-2 W BRAKER LN AUSTIN TX 78759
1	KAMAN SCIENCES CORP D L JONES 2560 HUNTINGTON AVE SUITE 200 ALEXANDRIA VA 22303
1	KAMAN SCIENCES CORP J S WILBECK 600 BLVD S SUITE 208 HUNTSVILLE AL 35802
1	ORLANDO TECHNOLOGY INC D A MATUSKA PO BOX 855 SHALIMAR FL 32579

<u>NO. OF COPIES</u>	<u>ORGANIZATION</u>
2	SRI INTERNATIONAL DR L SEAMAN DR D CURRAN 333 RAVENSWOOD AVE MENLO PARK CA 94025
3	TELEDYNE BROWN ENGR J W BOOTH M B RICHARDSON PO BOX 070007 MS 50 HUNTSVILLE AL 35807-7007
	<u>ABERDEEN PROVING GROUND</u>
19	DIR, USARL AMSRL-WM, I. MAY AMSRL-WM-T, W. F. MORRISON AMSRL-WM-TA, J. DEHN W. A. GOOCH H. W. MEYER AMSRL-WM-TC, K. KIMSEY D. SCHEFFLER AMSRL-WM-PD, G. GAZONAS AMSRL-WM-WD, A. PRAKASH AMSRL-WM-MF, A RAJENDRAN (5 CP) D GROVE (5 CP)
5	DIR, USARL AMSRL-WM-TD, A M DIETRICH M RAFTENBERG G RANDERS-PEHRSON M SCHEIDLER T WRIGHT

NO. OF
COPIES ORGANIZATION

1 ABTEILUNG FUER
PHYSIKALISCHE CHEMIE
MONT ANUNIVERSITAET
E KOENIGSBERGER
A 8700 LOEBEN
AUSTRIA

2 AWE
M GERMAN
W HARRISON
FOULNESS ESSEX SS3 9XE
UNITED KINGDOM

1 BATTELLE INGENIEUTECHNIK
GMBH
DUESSELDORFFER STR 9
ESCHBORN D 65760
GERMANY

1 BHABHA ATOMIC RESEARCH
CENTRE
HIGH PRESSURE PHYSICS
DIVISION
N SURESH
TROMBAY BOMBAY 400 085
INDIA

1 BULGARIAN ACADEMY OF
SCIENCES
SPACE RESEARCH INSTITUTE
VALENTIN GOSPODINOV
1000 SOFIA PO BOX 799
BULGARIA

1 CANADIAN ARSENALS LTD
P PELLETIER
5 MONTEE DES ARSENAUX
VILLIE DE GRADEUR PQ J5Z2
CANADA

1 CEA
R CHERET
CEDEX 15
313 33 RUE DE LA FEDERATION
PARIS 75752
FRANCE

NO. OF
COPIES ORGANIZATION

1 CEA
CISI BRANCH
P DAVID
CENTRE DE SACLAY BP 28
GIF SUR YVETTE 91192
FRANCE

1 CEA/CESTA
A GEILLE
BOX 2 LE BARP 33114
FRANCE

3 CENTRE D'ETUDES DE GRAMAT
S GERARD
C LOUPIAS
PASCALE OUTREBON
GRAMAT 46500
FRANCE

2 CENTRE D'ETUDES DE
LIMEIL-VALENTON
C AUSSOURD
J BOZIER
S G CEDEX
VILLENEUVE 94195
FRANCE

3 CENTRE D'ETUDES DE VAUJOURS
P JEAN-PAUL
E BOTTET
TAT SIHN VONG
BOITE POSTALE NO 7
COUNTRY 77181
FRANCE

1 CENTURY DYNAMICS LTD
N FRANCIS
12 CITY BUSINESS CTR
BRIGHTON RD HORSHAM
WEST SUSSEX RH1354BA
UNITED KINGDOM

1 CRC RESEARCH INST INC
M KATAYAMA
STRUCTURAL ENGINEERING DEPT
1 3 316 NAKASE MIHAMA KU
CHIBA SHI 261 01
JAPAN

NO. OF
COPIES ORGANIZATION

1 DAT ETBS CETAM
C ALTMAYER
ROUTE DE GUERRY BOURGES
18015
FRANCE

1 DEFENCE RESEARCH AGENCY
W A J CARSON
CHOBHAM LANE CHERTSEY
SURREY KT16 0EE
UNITED KINGDOM

1 DEFENCE RSCH ESTAB SUFFIELD
D MACKAY
RALSTON ALBERTA TOJ 2NO
RALSTON
CANADA

1 DEFENCE RSCH ESTAB SUFFIELD
C WEICKERT
BOX 4000 MEDICINE HAT
ALBERTA T1A 8K6
CANADA

1 DEFENCE RSCH ESTAB
VALCARTIER
N GASS
PO BOX 8800
COURCELETTE PQ GOA IRO
CANADA

4 DEPARTAMENTO DE QUIMICA FISICA
FACULTAD DE CIENCIAS QUIMICAS
UNIVERSIDAD COMPLUTENSE DE
MADRID
V G BAONZA
M TARAVILLO
M CACERAS
J NUNEZ
28040 MADRID
SPAIN

1 DYNAMIC RESEARCH AB
A PERSSON
PARADISGRAND 7
SODERTALJE S 151 36
SWEDEN

NO. OF
COPIES ORGANIZATION

4 ERNST MACH INSTITUT
VOLKER HOHLER
E SCHMOLINSKE
E SCHNEIDER
A J STILP
ECKERSTRASSE 4
D-7800 FREIBURG I BR 791 4
GERMANY

1 ESTEC CS
D CASWELL
BOX 200 NOORDWIJK
2200 AG
NETHERLANDS

1 EUROPEAN SPACE AGENCY
W FLURY
ESOC 5
ROBT BOSCHT STRASSE
DARMSTADT 6100
GERMANY

2 EUROPEAN SPACE AGENCY
ESTEC
L BERTHOUD
M LAMBERT
POSTBUS BOX 299 NOORDWIJK
NL2200 AG
NETHERLANDS

1 FRENCH GERMAN RESEARCH
INST
H F LEHR
POSTFACH 1260
WEIL AM RHEIN D-79574
GERMANY

3 FRENCH GERMAN RESEARCH INST
H ERNST
F JAMET
PASCALE LEHMANN
CEDEX 5 5 RUE DU GENERAL
ASSAGNOU
SAINT LOUIS 68301
FRANCE

<u>NO. OF</u> <u>COPIES</u>	<u>ORGANIZATION</u>	<u>NO. OF</u> <u>COPIES</u>	<u>ORGANIZATION</u>
4	HIGH ENERGY DENSITY RESEARCH CTR V E FORTOV G I KANEL V A SKVORTSOV O YU VOJOBIEV IZHORSKAJA STR 13/19 MOSCOW 127412 RUSSIAN REPUBLIC	1	IPE RAS A A BOGOMAZ DVORTSOVAIA NAB 18 ST PETERSBURG RUSSIAN REPUBLIC
5	IABG H J RAATSCHEN W SCHITTKE F F SCHARPPF M BORRMANN H G DORSCH EINSTEINSTRASSE 20 D 8012 OTTOBRUN B MUENCHEN GERMANY	1	ISL CHANTERET PIERRE-YVES F68301 SAINT-LOUIS CEDEX 12 RUE DE L'INDUSTRIE BP 301 FRANCE
1	INSTITUTE FOR PROBLEMS OF STRENGTH G STEPANOV TIMIRYAZEVSKEYU STR 2 252014 KIEV UKRAINE	1	LABORATOIRE DE TECHNOLOGIE DES SURFACES ECOLE CENTRALE DE LYON P VINET BP 163 69131 ECULLY CEDEX FRANCE
1	INSTITUTE OF CHEMICAL PHYSICS A YU DOLGOBORODOV KOSYGIN ST 4 V 334 MOSCOW	2	LAVRENTYEV INST. HYDRODYNAMICS L A MERZHIEVSKY V V SILVESTROV NOVOSIBIRSK 630090 RUSSIAN REPUBLIC
3	INSTITUTE OF CHEMICAL PHYSICS RUSSIAN ACADEMY OF SCIENCES A M MOLODETS S RAZORENOV A V UTKIN 142432 CHERNOGOLOVKA MOSCOW REGION RUSSIAN REPUBLIC	1	MOSCOW INST OF PHYSICS & TECH S V UTUZHNIKOV DEPT OF COMPUTATIONAL MATHEMATICS DOLGOPRUDNY 1471700 RUSSIAN REPUBLIC
2	IOFFEPHYSICO TECHNICAL INST DENSE PLASMA DYNAMICS LABORATORY E M DROBYSHEVSKI A KOZHUSHKO ST PETERSBURG 194021 RUSSIAN REPUBLIC	1	NATL DEFENCE DENSITY RSCH CTR J FORSS FOA FOX 551 TUMBA S 14725 SWEDEN
		3	NATL DEFENCE RESEARCH EST L HOLMBERG ULF LINDEBERG LARS GUNNAR OLSSON FOA BOX 551 TUMBA S 14725 SWEDEN

<u>NO. OF</u> <u>COPIES</u>	<u>ORGANIZATION</u>	<u>NO. OF</u> <u>COPIES</u>	<u>ORGANIZATION</u>
1	PML TNO E VAN RIET BOX 45 RIJSWIJK 2230AA NETHERLANDS	1	TECHNISCHE UNIVERSITAT MUENCHEN E B IGENBERGS RICHARD WAGNER STR 18 111 MUENCHEN 2 D8000 GERMANY
1	PRB S A M VANSNICK AVENUE DE TERVUEREN 168 BTE 7 BRUSSELS B 1150 BELGIUM	1	TOMSK BRANCH OF THE INST FOR STRUCTURAL MACROKINETICS V GORELSKI 8 LENIN SQ GSP 18 TOMSK 634050 RUSSIAN REPUBLIC
1	PRINS MAURITS LABORATORY H J REITSMA TNO BOX 45 RIJSWIJK 2280AA NETHERLANDS	1	TU CHEMNITZ-ZWICKAU L MEYER FAKULTAET FUER MASCHINENBAU U. VERFAHRENSTECHNIK SCHEFFELSTRASSE 110 09120 CHEMNITZ GERMANY
1	RAFAEL BALLISTICS CENTER DR Z ROSENBERG PO BOX 2250 HAIFA 31021 ISRAEL	1	UK MINISTRY OF DEFENCE G J CAMBRAY CBDE PORTON DOWN SALISBURY WITTSHERE SPR OJQ UNITED KINGDOM
1	RESEARCH INSTITUTE OF MECHANICS NIZHNIY NOVGOROD STATE UNIVERSITY A SADYRIN P R GAYARINA 23 KORP 6 NIZHNIY NOVGOROD 603600 RUSSIAN REPUBLIC	1	UNIVERSIDAD DE CANTABRIA FACULTAD DE CIENCIAS DEPARTAMENTO DE FISICA APLICADA J AMOROS AVDA DE LOS CASTROS S/N SANTANDER SPAIN
1	ROYAL ARMAMENT R&D ESTAB I CULLIS FORT HALSTEAD SEVENOAKS KENT TN14 7BJ UNITED KINGDOM	1	UNIVERSIDAD DE OVIEDO FACULTAD DE QUIMICA DEPARTAMENTO DE QUIMICA FISICA Y ANALITICA E FRANCISCO AVENIDA JULIAN CLAVERIA S/N 33006 - OVIEDO SPAIN
1	SAMARA STATE AEROSPACE UNIV L G LUKASHEV SAMARA RUSSIAN REPUBLIC		

NO. OF
COPIES ORGANIZATION

- 1 UNIVERSITY OF GUELPH
PHYSICS DEPT
C G GRAY
GUELPH ONTARIO
N1G 2W1
CANADA

- 2 UNIVERSITY OF KENT
UNIT FOR SPACE SCIENCES
PHILIPPE GENTA
PAUL RATCLIFF
CANTERBURY KENT CT2 7NR
UNITED KINGDOM

REPORT DOCUMENTATION PAGE			Form Approved OMB No. 0704-0188	
Public reporting burden for this collection of information is estimated to average 1 hour per response, including the time for reviewing instructions, searching existing data sources, gathering and maintaining the data needed, and completing and reviewing the collection of information. Send comments regarding this burden estimate or any other aspect of this collection of information, including suggestions for reducing this burden, to Washington Headquarters Services, Directorate for Information Operations and Reports, 1215 Jefferson Davis Highway, Suite 1204, Arlington, VA 22202-4302, and to the Office of Management and Budget, Paperwork Reduction Project(0704-0188), Washington, DC 20503.				
1. AGENCY USE ONLY (Leave blank)	2. REPORT DATE June 1997	3. REPORT TYPE AND DATES COVERED Final, Oct 95 - Sep 96		
4. TITLE AND SUBTITLE Analysis of Projectile Penetration Into a SiC/Ti Layered Plate			5. FUNDING NUMBERS 6MPCER	
6. AUTHOR(S) A. M. Rajendran, D. J. Grove, and K. D. Bishnoi*				
7. PERFORMING ORGANIZATION NAME(S) AND ADDRESS(ES) U.S. Army Research Laboratory ATTN: AMSRL-WM-MF Aberdeen Proving Ground, MD 21005-5069			8. PERFORMING ORGANIZATION REPORT NUMBER ARL-TR-1364	
9. SPONSORING/MONITORING AGENCY NAMES(S) AND ADDRESS(ES)			10. SPONSORING/MONITORING AGENCY REPORT NUMBER	
11. SUPPLEMENTARY NOTES *U.S. Army Tank Automotive Research, Development, and Engineering Center, Warren, MI 48397-5000				
12a. DISTRIBUTION/AVAILABILITY STATEMENT Approved for public release; distribution is unlimited.			12b. DISTRIBUTION CODE	
13. ABSTRACT (Maximum 200 words) This report describes the capabilities of the Rajendran-Grove ceramic model in predicting the depth of penetration in several layered ceramic targets. There are nine constants in the model. Five constants are adequate to describe the effects of microcracking on strength and stiffness. The variation of strength of the pulverized ceramic with respect to pressure is described through two constants. The plastic strain description involves two parameters that can be determined from a maximum stress vs. strain rate plot. A methodology to estimate these model constants is outlined in this report. Experimental data from high-velocity plate impact tests and a penetration test were employed in the calibration of the model constants for silicon carbide. Using this set of constants, the penetration of a solid tungsten rod into a layered ceramic target was analyzed. The target configuration consisted of a silicon carbide frontplate glued to a titanium backplate. The analysis showed that the simulated penetration resistance of the layered configuration was significantly influenced by the form of the ceramic model's pulverized strength equation. In addition, maintaining constant areal density, we examined the effects of different substrate materials (titanium, steel, and aluminum) on the calculated depths of penetration.				
14. SUBJECT TERMS ceramic failure model, ballistic penetration, pulverized strength model, depth of penetration, layered target			15. NUMBER OF PAGES 39	
			16. PRICE CODE	
17. SECURITY CLASSIFICATION OF REPORT UNCLASSIFIED	18. SECURITY CLASSIFICATION OF THIS PAGE UNCLASSIFIED	19. SECURITY CLASSIFICATION OF ABSTRACT UNCLASSIFIED	20. LIMITATION OF ABSTRACT UL	

INTENTIONALLY LEFT BLANK.

USER EVALUATION SHEET/CHANGE OF ADDRESS

This Laboratory undertakes a continuing effort to improve the quality of the reports it publishes. Your comments/answers to the items/questions below will aid us in our efforts.

1. ARL Report Number/Author ARL-TR-1364 (Rajendran) Date of Report June 1997

2. Date Report Received _____

3. Does this report satisfy a need? (Comment on purpose, related project, or other area of interest for which the report will be used.) _____

4. Specifically, how is the report being used? (Information source, design data, procedure, source of ideas, etc.) _____

5. Has the information in this report led to any quantitative savings as far as man-hours or dollars saved, operating costs avoided, or efficiencies achieved, etc? If so, please elaborate. _____

6. General Comments. What do you think should be changed to improve future reports? (Indicate changes to organization, technical content, format, etc.) _____

CURRENT
ADDRESS

Organization

Name

E-mail Name

Street or P.O. Box No.

City, State, Zip Code

7. If indicating a Change of Address or Address Correction, please provide the Current or Correct address above and the Old or Incorrect address below.

OLD
ADDRESS

Organization

Name

Street or P.O. Box No.

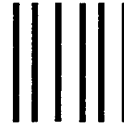
City, State, Zip Code

(Remove this sheet, fold as indicated, tape closed, and mail.)

(DO NOT STAPLE)

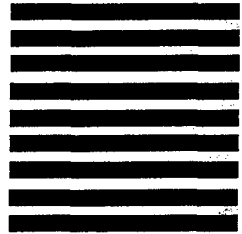
DEPARTMENT OF THE ARMY

OFFICIAL BUSINESS



NO POSTAGE
NECESSARY
IF MAILED
IN THE
UNITED STATES

BUSINESS REPLY MAIL
FIRST CLASS PERMIT NO 0001,APG,MD



POSTAGE WILL BE PAID BY ADDRESSEE

DIRECTOR
US ARMY RESEARCH LABORATORY
ATTN AMSRL WM MF
ABERDEEN PROVING GROUND MD 21005-5069
